ACS APPLIED MATERIALS & INTERFACES

Research Article

www.acsami.org

Enhanced Photocatalytic Activity and Charge Carrier Dynamics of Hetero-Structured Organic–Inorganic Nano-Photocatalysts

Kamala K. Nanda,[†,‡] Smrutirekha Swain,[†,‡] Biswarup Satpati,[§] Laxmidhar Besra,[†,‡] Biswajit Mishra,[†] and Yatendra S. Chaudhary*[,†,‡]

[†]Colloids and Materials Chemistry Department, CSIR-Institute of Minerals and Materials Technology, Bhubaneswar 751 013, India

[‡]Academy of Scientific and Innovative Research (CSIR-AcSIR), New Delhi 110 025, India

[§]Surface Physics and Material Science Division, Saha Institute of Nuclear Physics, 1/AF, Bidhannagar, Kolkata 700 064, India

Supporting Information

ABSTRACT: P3HT-coupled CdS heterostructured nanophotocatalysts have been synthesized by an inexpensive and scalable chemical bath deposition approach followed by drop casting. The presence of amorphous regions corresponding to P3HT in addition to the lattice fringes [(002) and (101)] corresponding to hexagonal CdS in the HRTEM image confirm the coupling of P3HT onto CdS. The shift of π^* (C═C) and σ^* (C−C) peaks toward lower energy losses and prominent presence of σ^* (C−H) in the case of P3HT−CdS observed in electron energy loss spectrum implies the formation of heterostructured P3HT−CdS. It was further corroborated by the shifting of S 2p peaks toward higher binding energy (163.8 and 164.8 eV) in the XPS spectrum of P3HT−CdS. The current density recorded under illumination for the 0.2 wt % P3HT−CdS photoelectrode is 3 times higher than that of unmodified CdS and other loading concentration of P3HT coupled CdS photoelectrodes. The solar hydrogen generation studies show drastic enhancement in the hydrogen generation rate i.e. 4108 μmol h^{-1} g^{-1} in the case of 0.2 wt % P3HT−CdS. The improvement in the photocatalytic activity of 0.2 wt % P3HT−CdS photocatalyst is ascribed to improved charge separation lead by the unison of shorter lifetime (τ_1 = 0.25 ns) of excitons, higher degree of band bending, and increased donor density as revealed by transient photoluminescence studies and Mott−Schottky analysis.

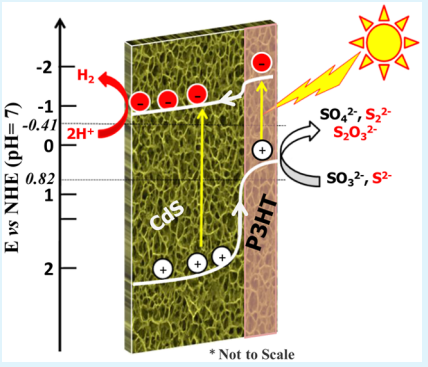

KEYWORDS: *photoelectrochemical water splitting, heterostructure, photocatalysis, time-resolved photoluminescence*

1. INTRODUCTION

Converting solar radiation into energy and storing it for later use in an economically viable way is the major challenge in the quest to replace fossil fuels with renewable energy. An integrated electrochemical system to generate oxygen and hydrogen (an energy carrier) via splitting water using solar radiation is one of the promising approaches to mimic photosynthesis. A variety of electrocatalysts/photocatalysts (ranging from semiconducting to supramolecular, viz., metal oxides, nitrides, phosphides, sulfides; Pt- and ruthenium complexes) are being explored for solar water splitting, but their overall efficiency is limited.[1−12] Such limitation of the efficiency is mainly due to the poor control over the recombinations of photogenerated charge carriers (excitons).[13] The conversion of photons into electrons (e^-) in a photocatalyst comprise of intriguing elemental processes such as light absorption, charge migration, charge separation, recombination, and fast excitons transport to the catalytic site. To tune these processes, we adopted the "bulk-heterojunction" strategy for organic photovoltaic (OPV), in which a mixture of donors (viz., regioregular poly(3-hexylthiophene) (P3HT) and acceptors (viz. (6,6) phenyl C61 butyric acid methyl ester (PCBM)) are used to increase donor−acceptor interface and enhance exciton dissociation.[14] Despite the exploration of a range of organic photocatalyst for solar hydrogen generation, both the efficiency and stability achieved are inferior to those observed for inorganic semiconducting photocatalysts.[12,15−17]

An alternative approach is to integrate organic and inorganic materials to design heterostructured photocatalysts. Such heterostructure imparts the synergized properties such as high charge carrier mobility, high absorption coefficient in visible light, and high dielectric permittivity (reduces the charge separation distance at the interface), arising from both the organic and inorganic counterparts, respectively. Which, in turn, may lead to improved charge separation at the heterointerface and reduces the geminate recombination probability.[18,19] Nonetheless, there are few reports on the development of heterostructured photocatalyst based on organic−inorganic heterojunction.[20−23]

To take advantage of the properties associated with organic hole transporting polymer and inorganic semiconductor, we have coupled P3HT onto CdS to form heterostructured

Received: January 2, 2015
Accepted: March 30, 2015
Published: March 30, 2015

DOI: 10.1021/acsami.5b00022
ACS Appl. Mater. Interfaces 2015, 7, 7970−7978

photocatalyst. The detailed studies on the charge carrier dynamics and its correlation with the photoelectrocatalytic water splitting and photocatalytic hydrogen generation activity have been undertaken. P3HT is semicrystalline, tends to form lamellar structure, and thus may lead to enhancement of the charge transport and hole mobility up to 0.1 $cm^2\ V^{-1}\ s^{-1}$.[22] It also has an absorption edge toward the red region of the solar spectrum, matching with that of photosystem-II and enabling it to absorb a broad range of solar radiation. On the other hand, CdS has an appropriate band energetics with P3HT to form donor−acceptor heterostructured photocatalyst. The coupling of CdS with P3HT may give rise to a heterointerface that may lead to enhancement of the exciton dissociation and charge collection processes. In addition, it is also expected to inhibit the photocorrosion of the CdS by its known hole (h^+) transporting property. In this study, we report the facile synthesis of P3HT-modified CdS heterostructured photocatalyst and its potential application in the photoelectrochemical water splitting reaction and photocatalytic hydrogen generation. The detailed results on the structure of the heterostructured photoelectrodes, their photocatalytic activity, solar H_2 generation efficiency, and charge carrier dynamics investigated using HRTEM, electron energy loss spectroscopy, X-ray photoelectron spectroscopy, time-resolved photoluminescence spectroscopy, carrier density, and Mott−Schottky analysis are presented.

2. EXPERIMENTAL SECTION

Indium tin oxide (ITO, SPI Supplies) was used as substrate for depositing cadmium sulfide (CdS) thin films. Cadmium nitrate tetra hydrate and thiourea used for the synthesis of CdS and chloroform were obtained from Merck. Poly(3-hexylthiophene-2,5-dilyl) (P3HT) was obtained from Aldrich.

2.1. Synthesis of CdS Thin Films. To grow CdS thin film, we first cleaned ITO substrate with acetone/isopropyl alcohol/deionized water. Then, 1.2 mL of 1 M cadmium nitrate solution was taken in a reaction vessel and mixed with 0.2 mL of ethanolamine (EA) to form a stable and clear Cd-EA complex solution. The pH of the resulting solution was measured using pH meter and found to be ∼10.78. Then 1.2 mL of 1 M thiourea was added to this reaction mixture. The reaction vessel was heated at 85 °C. A precleaned ITO glass substrate (1.5 × 1.2 cm) was dipped into the reaction solution at an angle so that its conducting side faced downward, and the thin film was allowed to grow for 40 min. The CdS deposited ITO was taken out from the reaction vessel and subjected to thorough washing with deionized water, and subsequently allowed to dry at 80 °C.

2.2. Preparation of P3HT Solution. Four different concentrations of P3HT solution (1, 2, 5, and 10 mg mL^{-1}) were prepared by adding appropriates amount of P3HT to 5 mL of chloroform and stirring overnight. A dark orange color solution was obtained.

2.3. Fabrication of Heterostructured Films. Approximately 0.2 mL of P3HT solutions were drop casted separately onto presynthesized CdS thin films and allowed to dry under ambient conditions.

2.4. Structural Characterization. To explore nano structural information, samples were subjected to transmission electron microscopy (TEM) investigation, carried out using an FEI Tecnai G2 F30, S-Twin microscope operating at 300 kV. The TEM is equipped with a scanning unit and a high-angle annular dark-field (HAADF) detector from Fischione (model 3000). Electron energy loss spectroscopy (EELS) was carried out using a post column Gatan Quantum SE (model 963 SE) in the same microscope. The sample was dispersed in ethanol using ultrasonic bath, mounted on a carbon coated Cu grid, dried, and used for TEM measurements. X-ray photoelectron spectrometry (XPS) measurements were carried out using multichamber XPS (PREVAC, Poland). All the binding energies were calculated keeping C 1s peak at 284.6 eV of the surface adventitious carbon as a reference.

2.5. Optical Properties (Band Gap Energy). The optical properties (band gap, E_g) were examined using a UV−vis spectrophotometer (UV-2450 SHIMADZU).

2.6. Photoluminescence Studies. Steady state emission of P3HT−CdS thin films were recorded using Edinburgh, FLS 980 Fluorescence spectrometer. Time-resolved photoluminescence decay measurements were carried out using a time-correlated single-photon counting (TCSPC) spectrometer (Edinburgh, FLS 980). A diode laser (470 nm) was used as the excitation source, and a photomultiplier (Hamamatsu R928P) was used as the detector (response time 120 ps). The IRF was recorded by scattering solution (dilute Ludox solution in water) in place of the sample. Time-resolved photoluminescence decay profiles were analyzed by nonlinear least-squares iteration procedures using FLS 980 decay analysis software using eq 1 The quality of the fit is accessed by the chi-square (χ^2) values between 1 and 1.3 and distribution of residuals.

$$\text{Fit} = A_1 + B_1 e^{(-t/\tau_1)} + B_2 e^{(-t/\tau_2)} + B_3 e^{(-t/\tau_3)} \quad (1)$$

2.7. Photoelectrocatalysis. To undertake the photoelectrochemical studies, CdS thin films and P3HT modified CdS thin films were converted into electrode by making ohmic contact with Cu wire using silver paint and epoxy. An aqueous solution containing 0.1 M Na_2S and 0.14 M Na_2SO_3 (pH ∼ 12.4) was used as an electrolyte, unless otherwise mentioned. The photoelectrochemical behavior of these photocatalyst samples was studied using a potentiostat (Princeton Applied Research). Ag/AgCl and Pt were used as a reference and counter electrode, respectively. A monochromator consisting 500 W xenon−mercury lamp was used as a light source to determine the IPCE (incident photon to current efficiencies) for unmodified and P3HT modified CdS. A 150 W Solar simulator (Hi-Tech) equipped with an AM1.5G filter was used as a light source for photoelectrochemical water splitting reaction. Mott−Schottky data was recorded using IVIUM electrochemical workstation at 1 kHz.

2.8. Photocatalytic Hydrogen Generation. The photocatalytic hydrogen production activities of unmodified and P3HT modified CdS photocatalyst were measured under illumination using 150 W Solar simulator (Hi-Tech) equipped with an AM 1.5G filter. The photocatalysts (scratched from the films) were dispersed in 0.1 M Na_2S and 0.14 M Na_2SO_3 solution (5 mL) taken in a photocatalytic cell. The solution in the cell was purged with nitrogen gas for 15 min to remove all the dissolved gases. The evolved gases were characterized using a PerkinElmer Clarus 480 gas chromatograph with a TCD detector. The room temperature was maintained at 25 °C.

3. RESULTS AND DISCUSSION

3.1. Structural Analysis of Heterostructured P3HT−CdS Thin Films. The XRD pattern recorded for CdS thin film exhibits the formation of hexagonal phase of CdS predominantly (Figure S1, Supporting Information). As shown in Figure 1A, the SEM image recorded for CdS thin film shows a porous network of interconnected thin flakes similar to the microstructure of a leaf (porous structure in natural leaf leads to enhancement of light harvesting up to 20% by internal reflection).[24] Such porous flaky structures are anticipated to provide high surface area and higher light harvesting for photocatalytic reactions. The partial filling of pores and thickening of walls of the CdS film can be seen in SEM image, implying the incorporation of P3HT (Figure 1B).

Furthermore, the structural information on unmodified and P3HT modified CdS thin film sample was investigated using TEM. A low magnification TEM image of CdS shows flakes consisting of interconnected CdS nanocrystals of the order of 7.10 ± 0.25 nm (Figure 2A). The concentric sharp rings in the selected area electron diffraction (SAED) pattern (Figure 2B) is a result of many small (nm) crystals and shows polycrystalline

DOI: 10.1021/acsami.5b00022
ACS Appl. Mater. Interfaces 2015, 7, 7970−7978

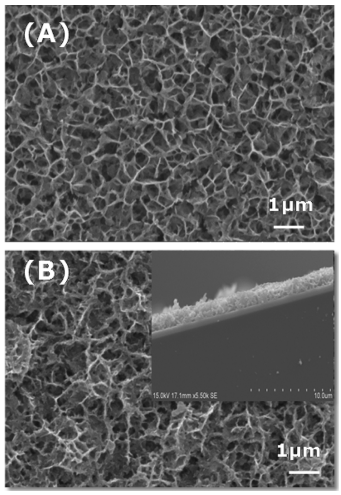

Figure 1. SEM image of (A) CdS thin film and (B) 0.2 wt % P3HT−CdS thin film; (inset) cross section of 0.2 wt % P3HT−CdS thin film.

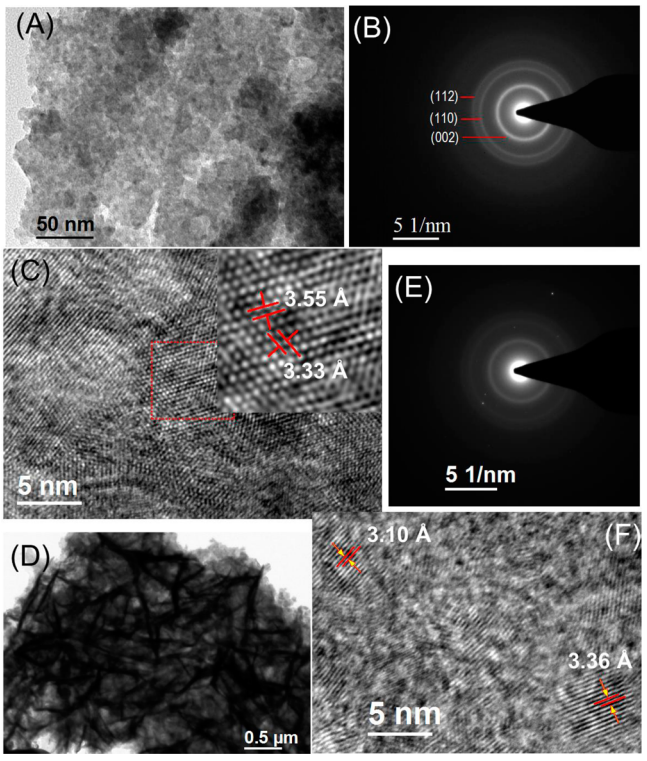

Figure 2. TEM analysis data for CdS film and 0.2 wt % P3HT−CdS film: (A and D) low-magnification images, (B and E) selected area diffraction patterns, and (C and F) high-resolution images. (C, inset) Fourier filtered image.

nature of the CdS thin film. The measured interplanar spacing (*d* spacing) from the SAED pattern are 3.36, 2.06, and 1.79 Å. These measured *d* spacings are very close to the (002), (110), and (112) interplanar spacings of hexagonal CdS (JCPDS # 80-0006). The lattice fringes for CdS thin film (Figure 2C) corresponds to (100) and (002) plane of the hexagonal phase of CdS. A low-magnification TEM image of P3HT modified CdS thin film sample, Figure 2D. The absence of distinct rings in the SAED pattern of heterostructured P3HT modified CdS thin film imply the incorporation of amorphous P3HT, Figure 2E. The grafting of P3HT was further confirmed by the presence of amorphous regions corresponding to P3HT in addition to the lattice fringes corresponding to hexagonal CdS in the HRTEM image of P3HT modified CdS thin film, Figure 2F.

The representative thin film samples (CdS, P3HT, and P3HT−CdS) were analyzed via electron energy loss spectroscopy (EELS) in an FEI Tecnai F30 TEM/STEM operating at 300 kV and equipped with a Gatan Model 693 Quantum imaging energy filter. Figure 3 shows high-angle annular dark-field scanning TEM (STEM-HAADF) image of three films and corresponding low-loss (left panel) and core-loss (right panel) EEL spectra. Zero loss peak was aligned on the CCD in imaging mode and then in spectroscopy mode and then in spectroscopy (left panel) and core-loss (right panel) EEL spectra. The full width at half-maximum intensity of the zero loss peaks after alignment was 1.2 eV. Collection aperture was 2.5 mm, and the energy dispersion was 0.05 and 0.25 eV for low-loss and core-loss, respectively. The probe size was about 2 nm. Volume plasmon measured from a macroscopic CdS particle in the spectroscopy mode of the Gatan Image Filter. The volume plasmon peak energy was measured to be 24.2 and 19.6 eV for CdS thin film, and the peak energy is shown as the dotted line through the graphs. The volume plasmon peak energy for macroscopic CdS particle was reported to be 18.5 ± 1 eV, and the measured plasmon energy was found to increase with decreasing particle size, which is in agreement with the theoretical approximation for plasmon shifting due to the quantum size effect.[25] Broadening of the peak is also observed, and it seems in proportion to the magnitude of the shifts. Two peaks observed here may be attributed to the CdS film subject to this study consisting of interconnected CdS nanocrystals of varying sizes. For P3HT film the plasmon peak energy is found to be 22.9 eV. For the P3HT−CdS film, the plasmon peak energy is found to be 22.9 and 23.8 eV. For the P3HT film, the reported plasmon peak energy is at 22.2 eV.[26] A shift to higher plasmon peak energy can be seen with decreasing particle size. The right panel of Figure 3 shows the stripped (stripped off the pre-edge background by fitting it to a power law) sulfur L2,3 edges at 165 eV overlapped with the carbon K edge at 284 eV and Cd M4,5 edges at 404 eV. In the case of P3HT−CdS film, the L2,3 edge of sulfur manifested changes in bonding structure. The EEL spectra recorded from C on grid, P3HT, and P3HT−CdS thin films on carbon coated film revealed the difference of the σ^* (C−H) peak in these three cases, while the shift of π^* (C═C) and σ^* (C−C) peaks toward lower energy losses was observed in the case of P3HT−CdS, implying the formation of heterostructured P3HT−CdS thin film (Figure 4.)[27]

To further understand the formation of heterostructure P3HT−CdS, X-ray photoelectron spectroscopy (XPS) analysis was carried out for the unmodified CdS, P3HT and heterostructured 0.2 wt % P3HT−CdS samples. The chemical shift of the S 2p peaks in the XPS spectrum for all samples was analyzed. Figure 5A shows S 2p peaks for unmodified P3HT thin film: S $2p_{3/2}$ (163.4 eV) and S $2p_{1/2}$ (164.2 eV) and is in agreement with the binding energy of S for P3HT.[22,28] The deconvolution of XPS spectra for P3HT−CdS sample shows the peaks corresponding to S 2p binding energies for CdS (161.8 and 163.2 eV)[29] and P3HT (163.8 and 164.8 eV) samples (Figure 5B). The shifting of S 2P peaks toward higher binding energy (163.8 and 164.8 eV) than that of observed for unmodified P3HT further corroborate the formation of heterostructured P3HT−CdS.

DOI: 10.1021/acsami.5b00022
ACS Appl. Mater. Interfaces 2015, 7, 7970−7978

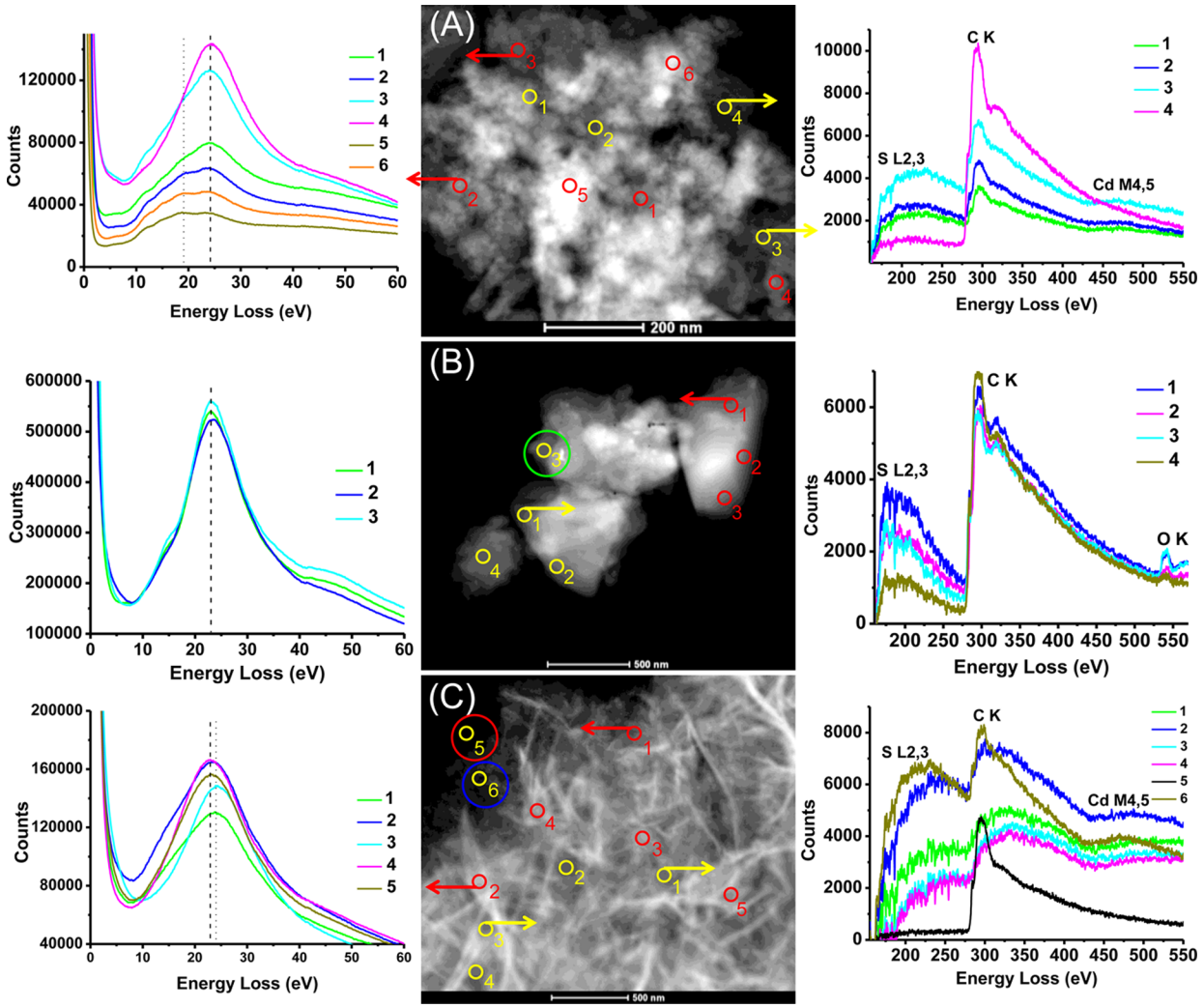

Figure 3. STEM-HAADF image of (A) CdS, (B) P3HT, and (C) P3HT−CdS films; (red O) positions used to collect low-loss spectra and (yellow O) points used to collect core-loss spectra. (Left) Low-loss spectra from these three films. (Right) Core-loss spectra from these three films.

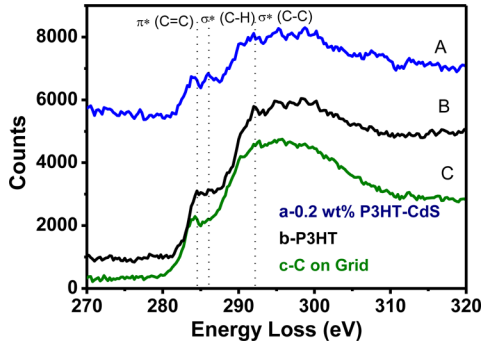

Figure 4. EELS fine structure of the carbon K-edge on P3HT and P3HT−CdS thin films.

3.2. Optical Properties (E_g) of Heterostructured P3HT−CdS Thin Films. The UV−vis absorption spectrum of bare P3HT shows a predominant absorption peak at 405 nm and a broadened peak at 592 nm (Figure 6A). The onset of this peak observed is at 673 nm. The red shift (∼15 nm) in the absorption maxima observed for heterostructured P3HT modified CdS films with respect to that of observed for bare P3HT film is indicative of e^- excitation from the valence band (VB) of P3HT to the conduction band (CB) of CdS. Similarly, when the concentration of P3HT loading increased from 0.1 wt % to 1 wt %, a red shift of the absorption edge is observed (Figure S2A, Supporting Information). The band gap (E_g), which determines the light harvesting efficacy of the photocatalyst, was determined for all samples from the reflectance data using Kubelka−Munk method (Figure 6B).[30] The unmodified CdS and P3HT show the E_g values of the order of 2.5 and 1.86 eV, respectively, which are in agreement with the values reported in the literature.[31,15] Upon coupling P3HT onto CdS thin films, the E_g value shows blue shift than that of observed for unmodified CdS thin film (Figure S2B, Supporting Information).

3.3. Photoelectrocatalysis Studies. To investigate the photoelectrocatalytic behavior of unmodified and P3HT modified CdS, linear sweep voltammograms (I−V) were recorded using an aqueous electrolyte solution containing 0.1 M Na_2S and 0.14 M Na_2SO_3 (pH ∼12.4) in a three electrode photoelectrochemical device. The unmodified and P3HT modified CdS photoelectrodes do not show significant current under dark until the breakdown potential is applied. When these photoelectrodes are exposed to visible light irradiation, a drastic enhancement in the anodic current density takes place in the case of 0.2 wt % P3HT−CdS (J_{an}: 0.65 mA cm^{-2} at 0.6 V vs NHE) (Figure 7B) and is higher than that of observed for

DOI: 10.1021/acsami.5b00022
ACS Appl. Mater. Interfaces 2015, 7, 7970−7978

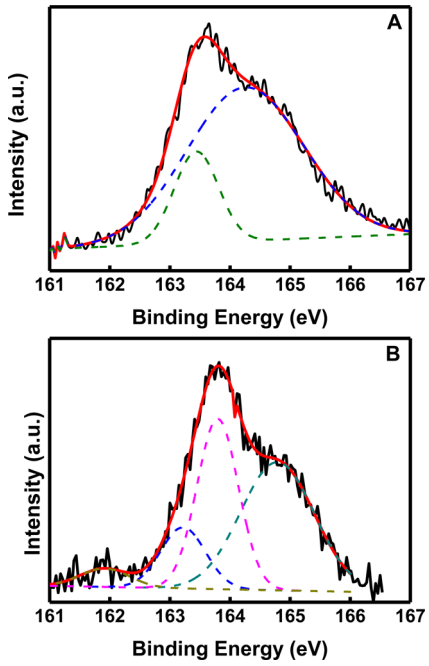

Figure 5. XPS spectra for S 2p (A) P3HT film and (B) heterostructured P3HT−CdS thin films.

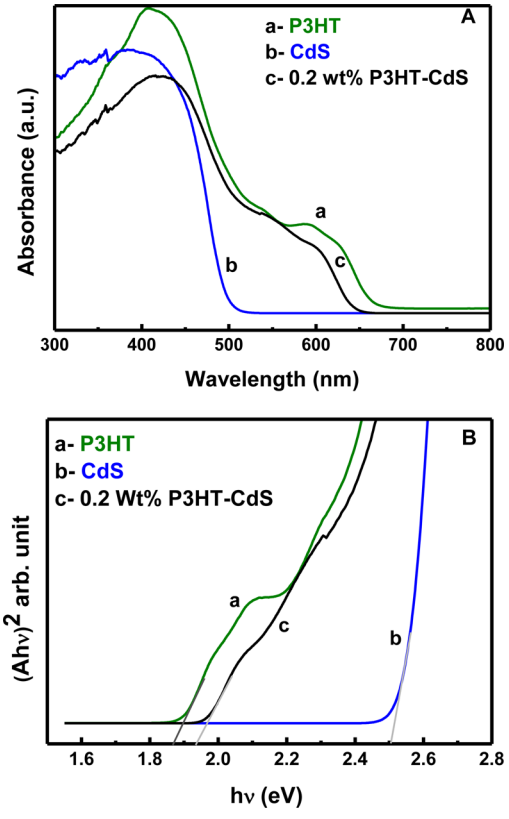

Figure 6. (A) Absorption spectra of P3HT, CdS, and heterostructured P3HT−CdS thin films. (B) Tau plot for P3HT, CdS, and heterostructured P3HT−CdS thin films.

unmodified CdS (J_{an}: 0.32 mA cm^{-2} at 0.6 V vs NHE), Figure 7A. As expected, unmodified P3HT does not exhibit any significant photocurrent. Among different concentrations (0.1, 0.2, 0.5, and 1.0 wt %) of P3HT used for coupling with CdS, 0.2 wt % P3HT−CdS shows higher current density under

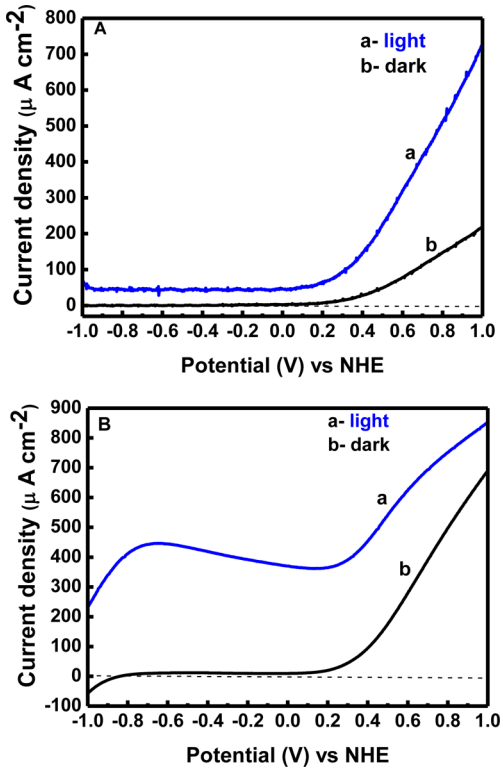

Figure 7. Current density of (A) CdS and (B) 0.2 wt % P3HT−CdS photoelectrodes recorded under dark and visible solar radiation in Na_2S/Na_2SO_3 electrolyte.

visible light irradiation than that of observed for 0.1 wt % P3HT−CdS (J_{an}: 0.11 mA cm^{-2} at 0.6 V vs NHE) and 1.0 wt % P3HT−CdS (J_{an}: 0.06 mA cm^{-2} at 0.6 V vs NHE) (Figure S3, Supporting Information). Although 0.5 wt % P3HT−CdS and 0.2 wt % P3HT−CdS thin film have comparable photocurrents, there is a greater quenching of fluorescence in 0.2 wt % P3HT−CdS implying reduced recombination of photogenerated charge carriers in the case of 0.2 wt % P3HT−CdS, Figure 8A.

3.4. Charge Carrier Dynamics in Heterostructured P3HT−CdS Photocatalysts. The charge separation of photogenerated excitons (photogenerated e^- and h^+) plays a vital role in efficient photoelectro-catalysis. To underpin the charge separation phenomena for the developed photoelectrodes, we performed steady-state and time-resolved photoluminescence studies. Figure 8A shows photoluminescence decay spectra of P3HT and heterostructured 0.2 wt % P3HT−CdS thin film, at λ_{ex}= 470 nm that the fluorescence of P3HT is quenched (>75%) when grafted onto CdS.

The 0.2 wt % P3HT−CdS photoelectrodes exhibit lower emission intensity and thereby higher quenching of the radiative recombinations of P3HT through an efficient e^- transfer from P3HT to CdS as compared to that of 0.5, 0.1, and 1 wt % P3HT modified CdS photoelectrodes. Similarly, quenching of fluorescence can be seen in the emission intensity of CdS in the heterostructured 0.2 wt % P3HT−CdS photoelectrode when the 350 nm excitation wavelength was used (corresponds to CdS; Figure S4A, Supporting Information). Such quenching of fluorescence observed is due to suppressed excitons recombination, implying the transfer of h^+ from the VB of CdS to the highest occupied molecular orbital (HOMO) of P3HT.[32,33] Figure 8B shows the photoluminescence decay for P3HT and 0.2 wt % P3HT−CdS

DOI: 10.1021/acsami.5b00022
ACS Appl. Mater. Interfaces 2015, 7, 7970−7978

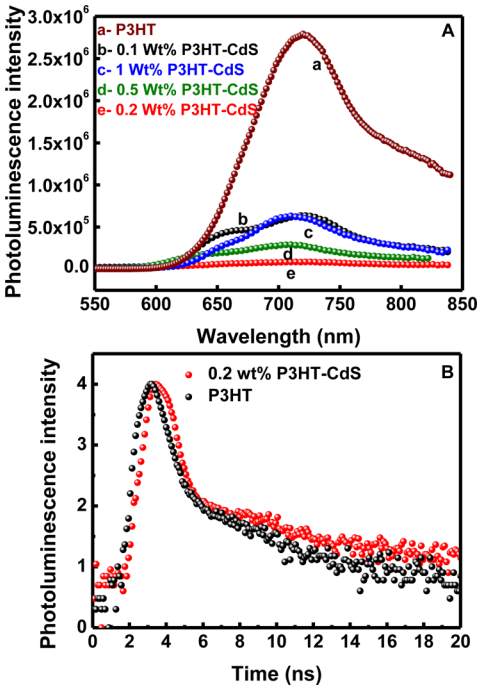

Figure 8. (A) Steady-state emission spectrum of P3HT and heterostructured P3HT−CdS thin films. (B) Time-resolved photoluminescence decay spectra of P3HT and heterostructured 0.2 wt % P3HT−CdS thin film, at λ_{ex}= 470 nm.

photoelectrodes. The higher value of photoluminescence lifetime (τ_1 = 0.41 ns) for 1 wt % P3HT−CdS in comparison to other loading concentration of P3HT onto CdS thin films may be attributed to the higher rate of charge carrier recombination (Table S1, Supporting Information). The shorter lifetime (τ_1 = 0.25 ns) in the case of 0.2 wt % P3HT−CdS thin films imply better charge separation occurring at the heterointerface of P3HT and CdS by providing a new nonradiative process for photogenerated excitons.[32] Decay fractions f_2 and f_3 are 0 in the case of all P3HT modified CdS photoelectrodes indicating the prevalence of nonradiative decay over radiative decay. It implies that better charge separation taking place in the case of 0.2 wt % P3HT−CdS is leading to better photoelectrocatalytic activity, and is in agreement with the improved photocurrent density observed for 0.2 wt % P3HT−CdS than that of other unmodified and P3HT modified CdS photoelectrodes.

To examine the carrier density (N_D) and flat band potential (V_{fb}), we conducted capacitance measurements at 1 kHz frequency. The N_D and V_{fb} values for photoelectrodes in sulfide−sulfite electrolyte were determined using Mott−Schottky equations.[34]

$$\frac{1}{C^2} = \frac{2}{\varepsilon\varepsilon_0 A^2 e N_D}\left(V - V_{fb} - \frac{k_\beta T}{e}\right) \quad (2)$$

where C and A represent the interfacial capacitance and area, respectively, N_D is the number of donors, V is the applied voltage, k_β is the Boltzmann's constant, T is the absolute temperature, and e is the electronic charge. The extrapolation of the linear part of the curves to $(1/C^2 = 0)$, gives the flat band potential of semiconductor. The values of flat band potentials under dark are given in Table 1. The N_D values were also

Table 1. Flat Band Potential and Carrier Density Values of Unmodified and Modified Thin Films

thin films	flat band potential (V vs NHE)	carrier density (cm^{-3})
CdS	−0.41	1.38×10^{26}
P3HT	−0.37	2.92×10^{26}
P3HT−CdS	−0.58	2.53×10^{27}

determined from the slope of the linear part of the Mott−Schottky plot using following equation for all samples.

$$\text{Slope} = \frac{2}{\varepsilon\varepsilon_0 A^2 e N_D} \quad (3)$$

The Mott−Schottky behavior is in accordance with the expected behavior of n-type semiconductor under increased anodic bias (Figure S5, Supporting Information). There is a sharp decrease in capacitance when the anodic bias is increased above the flat band potential.[35] The lower slope observed for 0.2 wt % P3HT−CdS implies higher N_D value that further corroborates with its improved photoelectrocatalytic activity (Figure S5, Supporting Information). The 0.2 wt % P3HT−CdS photoelectrode show higher N_D and more negative V_{fb} value, Table 1. The presence of hole scavenger (holes oxidizes SO_3^{2-} and S^{2-} to form SO_4^{2-} and S_2^{2-} species) appears to reduce photo-oxidation of P3HT further at photoelectrode−electrolyte interface, resulting in higher carrier densities and consequently higher photocurrent density.[36] In addition, the higher cathodic shift in V_{fb} value of 0.2 wt % P3HT−CdS signifies increased e^- density and thus higher degree of band bending. As a result the Fermi level of CdS in 0.2 wt % P3HT−CdS shifts toward the conduction band. The upward shift of Fermi level facilitate an improved charge separation at photoelectrode/electrolyte interface and thus lead to better photoelectrocatalytic activity in the case of 0.2 wt % P3HT−CdS.

3.5. Photostability and IPCE of Heterostructured P3HT−CdS Photocatalysts. The stability of photoelectrodes is one of the crucial aspects for their viable application in the water splitting. To evaluate the stability of unmodified CdS and 0.2 wt % P3HT modified CdS photoelectrodes, we performed chronoamperometric measurements in the sulfide−sulfite electrolyte, (Figure S6, Supporting Information). Even after 300 min of continuous illumination, a photocurrent many folds higher than that observed for unmodified CdS is retained. It implies reasonably good stability of heterostructured P3HT−CdS photoelectrode. In addition, the repeated (5 cycles) I−V measurements show no significant change in the photocurrent values, further confirming the photostability of heterostructured P3HT−CdS.

To estimate the quantitative correlation of light harvesting to exciton (photogenerated $e^-$and h^+) generation, we calculated the incident photon to current conversion efficiency (IPCE) or external quantum efficiency (EQE) for all samples at the wavelengths ranging from UV to visible solar radiation using the following equation (Figure 9).[37]

$$\text{IPCE}\ (\%) = \frac{1240 \times I_{ph}(\text{mA cm}^{-2})}{\lambda(\text{nm}) \times \text{PF}(\text{mW cm}^{-2})} \times 100 \quad (4)$$

For 0.2 wt % P3HT−CdS, IPCE keeps on increasing from ~8.91% at 600 nm to ~13.2% at 400 nm, using sulfide−sulphite electrolyte, Figure 9. This clearly shows that when CdS modified with P3HT, there is significant enhancement in the

DOI: 10.1021/acsami.5b00022
ACS Appl. Mater. Interfaces 2015, 7, 7970−7978

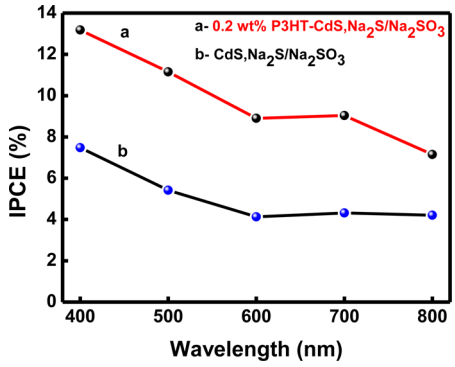

Figure 9. IPCE action spectra for (A) CdS and (B) 0.2 wt % P3HT−CdS photoelectrodes.

IPCE due to an efficient separation of photogenerated excitons at CdS−P3HT/electrolyte interface.

3.6. Photocatalytic Hydrogen Generation. In addition to the in-depth studies of the photoelectrocatalytic activities of unmodified and optimized P3HT modified CdS photocatalysts, the qualitative and quantitative photocatalytic H_2 evolution measurements under visible light were undertaken using the gas chromatograph. Among different loading concentrations of P3HT on CdS, the best performing 0.2 wt % P3HT−CdS was chosen to undertake photocatalytic hydrogen generation activity evaluation. The CdS and heterostructured 0.2 wt % P3HT−CdS photocatalyst amounts were optimized using 5 mL of sulfide−sulphite electrolyte. The rate of H_2 evolution for unmodified and P3HT modified CdS photocatalysts scratched from thin films is shown in Figure 10.

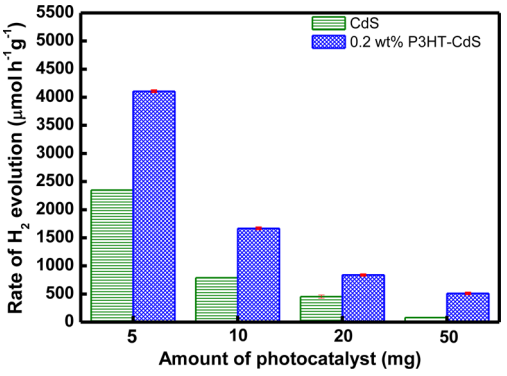

Figure 10. Photocatalytic hydrogen evolution rate for unmodified CdS and 0.2 wt % P3HT−CdS (8 h, 5 mL 0.1 M Na_2S−0.14 M Na_2SO_3, pH ∼ 12.4).

Unmodified CdS shows slower solar H_2 production (i.e., 2350 μmol h^{-1} g^{-1}), whereas the 0.2 wt % P3HT−CdS heterostructured photocatalyst shows faster photocatalytic hydrogen generation (i.e., 4108 μmol h^{-1} g^{-1}). It is many times faster than that of other P3HT-based heterostructures reported (4 μmol h^{-1} g^{-1} for gC_3N_4−P3HT heterojunction photocatalyst and 2000 μmol h^{-1} g^{-1} upon loading precious noble metals like Pt and/or Au) in the literature.[38,39]

A schematic showing the possible mechanism for the solar H_2 generation using heterostructured P3HT−CdS photocatalyst is shown in Figure 11. When the visible solar radiation falls on the P3HT−CdS photocatalyst, excitons are generated via photon absorption in both CdS and P3HT. This process is followed by the exciton diffusion to donor−acceptor interface.

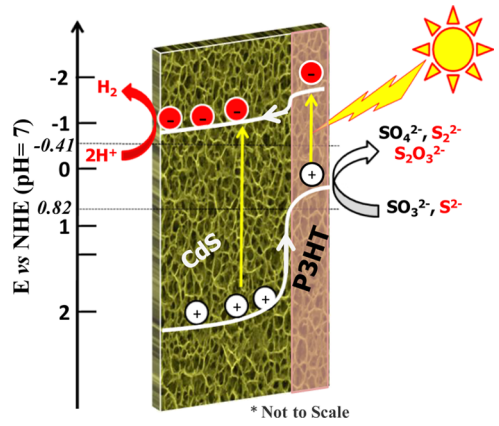

Figure 11. Schematic representation of the photocatalytic hydrogen generation on heterostructured photocatalysts.

Due to high electron affinity of CdS as compared to P3HT, the e^- gets drifted toward CdS leaving h^+ in P3HT followed by formation of charge transfer states. The h^+ from CdS VB diffuse into LUMO of P3HT inhibiting photocorrosion of CdS. Subsequently, the photogenerated e^- leads to the reduction of H^+ to H_2.

4. CONCLUSIONS

We have developed a simple chemical bath deposition method that leads to the reproducible formation of porous CdS thin films with a microstructure similar to that of a natural leaf. The modification of these thin films with optimized concentration of P3HT leads to a drastic improvement in the photocurrent density and enhancement in the photocatalytic hydrogen generation (4108 μmol $h^{-1}g^{-1}$). The improvement in the photocatalytic activity of 0.2 wt % P3HT coupled CdS photocatalyst is mainly due to the improved charge separation led by the heterointerface and appropriate energetics of the P3HT−CdS heterostructured photocatalyst. The modification of CdS with hole transporting polymer also show the improvement in the stability. These results suggest the potential candidature of hole transporting polymers for the modification of photocorrosive visible light active semiconductors to form heterostructured photocatalysts with improved solar hydrogen generation efficiency and stability. It also serves as an inspiration to fabricate other organic−inorganic heterostructured photocatalysts to surpass the recombinations problem such that an improved charge separation may be achieved to design efficient artificial photosynthesis devices.

■ ASSOCIATED CONTENT

Supporting Information

XRD pattern for CdS, absorbance and tau plot for P3HT and 0.1, 0.5, and 1.0 wt % P3HT−CdS thin films; current density data for 0.1, 0.5, and 1.0 wt % P3HT−CdS photoelectrodes under dark and illumination; steady state and time-resolved photoluminescence spectra for CdS and P3HT−CdS thin films; Mott−Schottky plots for P3HT, CdS, and P3HT−CdS photoelectrodes in polysulfide electrolytes and photo stability of CdS and P3HT−CdS photoelectrodes. This material is available free of charge via the Internet at http://pubs.acs.org.

DOI: 10.1021/acsami.5b00022
ACS Appl. Mater. Interfaces 2015, 7, 7970−7978

AUTHOR INFORMATION

Corresponding Author

*Fax: +91-674-2581637. Tel.:+91-674-2379248. E-mail: yschaudhary@immt.res.in.

Notes

The authors declare no competing financial interest.

ACKNOWLEDGMENTS

The authors are grateful to MNRE (103/155/2009-NT) and CSIR (NWP-56, YSP-04/2013), India, for financial assistance and to Prof. B. K. Mishra, Director, IMMT Bhubaneswar for providing the support to undertake this work. We also thank Mr. Shyamal Mondal, SINP, Kolkata, and Mr. Tapan Dash, CSIR-IMMT, Bhubaneswar for XPS measurements of samples.

REFERENCES

(1) Hitoki, G.; Takata, T.; Kondo, J. N.; Hara, M.; Kobayashi, H.; Domen, K. An Oxynitride, TaON, as an Efficient Water Oxidation Photocatalyst under Visible Light Irradiation ($\lambda \leq 500$ nm). *Chem. Commun.* **2002**, *16*, 1698−1699.

(2) Ishikawa, A.; Takata, T.; Kondo, J. N.; Hara, M.; Kobayashi, H.; Domen, K. Oxysulfide $Sm_2Ti_2S_2O_5$ as a Stable Photocatalyst for Water Oxidation and Reduction under Visible Light Irradiation ($\lambda \leq 650$ nm). *J. Am. Chem. Soc.* **2002**, *124*, 13547−13553.

(3) Maeda, K.; Takata, T.; Hara, M.; Saito, N.; Inoue, Y.; Kobayashi, H.; Domen, K. GaN:ZnO Solid Solution as a Photocatalyst For Visible-Light-Driven Overall Water Splitting. *J. Am. Chem. Soc.* **2005**, *127*, 8286−8287.

(4) Maeda, K.; Teramura, K.; Lu, D.; Takata, T.; Saito, N.; Inoue, Y.; Domen, K. Photocatalyst Releasing Hydrogen from Water. *Nature* **2006**, *440*, 295.

(5) Lee, Y.; Terashima, H.; Shimodaira, Y.; Teramura, K.; Hara, M.; Kobayashi, H.; Domen, K.; Yashima, M. Zinc Germanium Oxynitride as a Photocatalyst for Overall Water Splitting under Visible Light. *J. Phys. Chem. C* **2007**, *111*, 1042−1048.

(6) Liu, M.; Snapp, N. L.; Park, H. Water Photolysis with a Cross-Linked Titanium Dioxide Nanowire Anode. *Chem. Sci.* **2011**, *2*, 80−87.

(7) Esswein, A. J.; Nocera, D. G. Hydrogen Production by Molecular Photocatalysis. *Chem. Rev.* **2007**, *107*, 4022−4047.

(8) Ravelli, D.; Dondi, D.; Fagnoni, M.; Albini, A. Photocatalysis. A Multi-Faceted Concept for Green Chemistry. *Chem. Soc. Rev.* **2009**, *38*, 1999−2011.

(9) Kohl, S. W.; Weiner, L.; Schwartsburd, L.; Konstantinovski, L.; Shimon, L. J. W.; Ben-David, Y.; Iron, M. A.; Milstein, D. Consecutive Thermal H_2 and Light-Induced O_2 Evolution from Water Promoted by a Metal Complex. *Science* **2009**, *324*, 74−77.

(10) Kunkely, H.; Vogler, A. Water Splitting by Light with Osmocene as Photocatalyst. *Angew. Chem., Int. Ed.* **2009**, *48*, 1685−1687.

(11) Li, L.; Duan, L.; Xu, Y.; Gorlov, M.; Hagfeldtab, A.; Sun, L. A Photoelectrochemical Device for Visible Light Driven Water Splitting by a Molecular Ruthenium Catalyst Assembled on Dye-Sensitized Nanostructured TiO_2. *Chem. Commun.* **2010**, *46*, 7307−7309.

(12) Lanzarini, E.; Antognazza, M. R.; Biso, M.; Ansaldo, A.; Laudato, L.; Bruno, P.; Metrangolo, P.; Resnati, G.; Ricci, D.; Lanzani, G. Polymer-Based Photocatalytic Hydrogen Generation. *J. Phys. Chem. C* **2012**, *116*, 10944−10949.

(13) Kamat, P. V. Quantum Dot Solar Cells. Semiconductor Nanocrystals as Light Harvesters. *J. Phys. Chem. C* **2008**, *112*, 18737−18753.

(14) Dennler, G.; Scharber, M. C.; Brabec, C. J. Polymer-Fullerene Bulk-Heterojunction Solar Cells. *Adv. Mater.* **2009**, *21*, 1323−1338.

(15) El-Rashiedy, O. A.; Holdcroft, S. Photoelectrochemical Properties of Poly(3-alkylthiophene) Films in Aqueous Solution. *J. Phys. Chem.* **1996**, *100*, 5481−5484.

(16) Saito, K.; Kuwabara, J.; Kanbara, T. Photoelectrochemical Response of Poly(3-hexylthiophene) and Poly(2,3-diethylquinoxaline-5,8-diyl) in Aqueous Media. *Synth. Met.* **2011**, *161*, 1150−1153.

(17) Yang, S.; Yang, S. Photoelectrochemistry of Langmuir−Blodgett Films of the Endohedral Metallofullerene $Dy@C_{82}$ on ITO Electrodes. *J. Phys. Chem. B* **2001**, *105*, 9406−9412.

(18) Witt, E.; Witt, F.; Trautwein, N.; Fenske, D.; Neumann, J.; Borchert, H.; Parisi, J.; Olesiak, J. K. Synthesis of Lead Chalcogenide Nanocrystals and Study of Charge Transfer in Blends of PBSE Nanocrystals and Poly(3-hexylthiophene). *Phys. Chem. Chem. Phys.* **2012**, *14*, 11706−11714.

(19) Ehrler, B.; Walker, B. J.; Böhm, M. L.; Wilson, M. W. B.; Vaynzof, Y.; Friend, R. H.; Greenham, N. C. In Situ Measurement of Exciton Energy in Hybrid Singlet-Fission Solar Cells. *Nat. Commun.* **2012**, *3*, 1019.

(20) Zhang, H.; Zhu, Y. Significant Visible Photoactivity and Antiphotocorrosion Performance of CdS Photocatalysts after Monolayer Polyaniline Hybridization. *J. Phys. Chem. C* **2010**, *114*, 5822−5826.

(21) Liao, G.; Chen, S.; Quan, X.; Chen, H.; Zhang, Y. Photonic Crystal Coupled TiO_2/Polymer Hybrid for Efficient Photocatalysis under Visible Light Irradiation. *Environ. Sci. Technol.* **2010**, *44*, 3481−3485.

(22) Liang, H. C.; Li, X. Z. Visible-Induced Photocatalytic Reactivity of Polymer−Sensitized Titania Nanotube Film. *Appl. Catal., B* **2009**, *86*, 8−17.

(23) Xu, S.; Gu, L.; Kaihua; Yang, H.; Song, Y.; Jiang, L.; Dan, Y. The Influence of The Oxidation Degree of Poly(3-hexylthiophene) on The Photocatalytic Activity of Poly(3-hexylthiophene)/TiO_2 Composites. *Sol. Energy Mater. Sol. Cells.* **2012**, *96*, 286−291.

(24) Zhou, H.; Li, X.; Fan, T.; Osterloh, F. E.; Ding, J.; Sabio, E. M.; Zhang, D.; Guo, Q. Artificial Inorganic Leafs for Efficient Photochemical Hydrogen Production Inspired by Natural Photosynthesis. *Adv. Mater.* **2010**, *22*, 951−956.

(25) Nakashima, P. N. H.; Tsuzuki, T.; Johnson, A. W. S. Particle Size Dependence of the Volume Plasmon Energy in Cadmium Sulphide Quantum Dots by Electron Energy Loss Spectroscopy. *J. Appl. Phys.* **1999**, *85*, 1556−1559.

(26) Herzing, A.; Richter, L. J.; Anderson, I. M. 3D Nanoscale Characterization of Thin-Film Organic Photovoltaic Device Structures via Spectroscopic Contrast in the TEM. *J. Phys. Chem. C* **2010**, *114*, 17501−17508.

(27) Zheng, Y.; Jiao, Y.; Zhu, Y.; Li, L. H.; Han, Y.; Chen, Y. Hydrogen Evolution by a Metal-Free Electrocatalyst. Nature Communications. *Nat. Commun.* **2014**, *5*, 3783.

(28) Takemura, S.; Kato, H.; Nakajima, Y. Photoelectron Studies of Electrochemical Diffusion of Conducting Polymer/Transparent Conductive Metal Oxide Film Interfaces. *Appl. Surf. Sci.* **1999**, *144−145*, 360−365.

(29) NIST X-ray Photoelectron Spectroscopy Database; Measurement Services Division, National Institute of Standards and Technology: Gaithersburg, MD, 2003; http://srdata.nist.gov/xps/.

(30) Murphy, A. B. Band-Gap Determination from Diffuse Reflectance Measurements of Semiconductor Films and Application to Photoelectrochemical Water-Splitting. *Sol. Energy Mater. Sol. Cells.* **2007**, *91*, 1326−1337.

(31) Oliva, A. I.; Canto, O. S.; Rodrıguez, R. C.; Quintana, P. Formation of the Band Gap Energy on CdS Thin Films Growth by Two Different Techniques. *Thin Solid Films* **2001**, *391*, 28−35.

(32) Lin, Y. Y.; Chen, C. W.; Chu, T. H.; Su, W. F.; Lin, C. C.; Ku, C. H.; Wu, J. J.; Chen, C. H. Nanostructured Metal Oxide/Conjugated Polymer Hybrid Solar Cells by Low Temperature Solution Processes. *J. Mater. Chem.* **2007**, *17*, 4571−4576.

(33) Chasteen, S. V.; Carter, S. A.; Rumbles, G. Exciton Dynamics and Device Performance in Polythiophene Heterojunctions for Photovoltaics. *Proc. SPIE* **2005**, *5938*, 59380J1−59380J11.

(34) Gelderman, K.; Lee, L.; Donne, S. W. Flat-Band Potential of a Semiconductor: Using the Mott−Schottky Equation. *J. Chem. Educ.* **2007**, *84*, 685−688.

DOI: 10.1021/acsami.5b00022
ACS Appl. Mater. Interfaces 2015, 7, 7970−7978

(35) Baram, N.; Ein-Eli, Y. Electrochemical Impedance Spectroscopy of Porous TiO_2 for Photocatalytic Applications. *J. Phys. Chem. C* **2010**, *114*, 9781−9790.
(36) Bao, N.; Shen, L.; Takata, T.; Domen, K. Self-Templated Synthesis of Nanoporous CdS Nanostructures for Highly Efficient Photocatalytic Hydrogen Production under Visible Light. *Chem. Mater.* **2008**, *20*, 110−117.
(37) Chen, L.; Alarcón-Lladó, E.; Hettick, M.; Sharp, I. D.; Lin, Y.; Javey, A.; Ager, J. W. Reactive Sputtering of Bismuth Vanadate Photoanodes for Solar Water Splitting. *J. Phys. Chem. C* **2013**, *117*, 21635−21642.
(38) Yan, H.; Huang, Y. Polymer Composites of Carbon Nitride and Poly(3-hexylthiophene) to Achieve Enhanced Hydrogen Production from Water under Visible Light. *Chem. Commun.* **2011**, *47*, 4168−4170.
(39) Zhang, Y.; Mao, F.; Yan, H.; Liu, K.; Cao, H.; Wu, J.; Xiao, D. A Polymer−Metal−Polymer−Metal Heterostructure for Enhanced Photocatalytic Hydrogen Production. *J. Mater. Chem. A* **2015**, *3*, 109−115.

DOI: 10.1021/acsami.5b00022
ACS Appl. Mater. Interfaces 2015, 7, 7970−7978